Proceedings of the ASME 2010 3rd Joint US-European Fluids Engineering Summer Meeting and 8th International Conference on Nanochannels, Microchannels, and Minichannels
FEDSM-ICNMM2010
August 1-5, 2010, Montreal, Canada

FEDSM-ICNMM2010-30513

AN EFFICIENT FINITE ELEMENT PROCEDURE FOR THE ANALYSIS OF CROSS-FLOW MICRO HEAT EXCHANGERS

C. Nonino[*]**, S. Savino, S. Del Giudice**

Università degli Studi di Udine
Dipartimento di Energetica e Macchine
Via delle Scienze 208, 33100 Udine, Italy
Email: carlo.nonino@uniud.it

ABSTRACT

As an alternative to massive CFD, a hybrid technique, which has the advantage of accounting for all of the three-dimensional features of the flow field, but with a limited computational effort, is used for the solution of conjugate convection-conduction heat transfer problems in cross-flow micro heat exchangers. The key feature of the proposed method is represented by the separate computation of the velocity fields in single microchannels and on the subsequent mapping of such velocity fields onto the three-dimensional grid used to solve the thermal problem.

The cross-flow micro heat exchangers considered in the paper consist of a number of layers of rectangular microchannels. A parametric study is carried out on the combined effect on cross-flow micro heat exchanger thermal performances due to the variation of the microchannel cross-section and of the ratio of solid to fluid thermal conductivity.

NOMENCLATURE

c	specific heat [J/kg K]
D_h	hydraulic diameter [m]
H	height of the microchannel cross-section [m]
K	resistance coefficient [$-$]
k	thermal conductivity [W/m K]
$\dot{m}'$	mass flow rate per unit height [kg/m s]
n	outward normal to the boundary [m]
Pr	Prandtl number ($= c_f\mu_f/k_f$)
p	deviation from the hydrostatic pressure [Pa]
q'	heat flow rate per unit height [W/m]
Re	Reynolds number ($= \rho_f\overline{u}D_h/\mu_f$)
T	dimensionless temperature ($= (t - t_{c,i})/(t_{h,i} - t_{c,i})$)
t	temperature [°C]
u, v, w	velocity components in x, y and z directions [m/s]
W	width of the microchannel cross-section [m]
x, y, z	Cartesian coordinates [m]
γ	aspect ratio of the cross-section ($= H/W$)
ε	effectiveness [$-$]
ϕ	velocity correction potential [m^2/s]
μ	dynamic viscosity [kg/m s]
ρ	density [kg/m^3]

Subscripts and superscripts

b	bulk
c	cold fluid
f	fluid
i	inlet
h	hot fluid
max	maximum value
min	minimum value
o	outlet
ref	reference ($\gamma = 1$ and $\dot{m}' = \dot{m}'_1$)
s	solid
$-$	average value

[*]Address all correspondence to this author.

INTRODUCTION

In the analysis of the thermal performance of conventional size heat exchangers, the wall conduction effects can, in general, be neglected since the wall thickness is usually very small compared to the hydraulic diameter of the flow passages. On the contrary, in most microscale thermal devices, the area of the section of the solid material perpendicular to the flow direction is comparable to the area of the channel cross-section. Therefore, it has long been recognized that the thermal performances of microchannel heat exchangers and heat sinks are strongly affected by the coupling of the heat conduction taking place in the solid walls and of the forced convection inside the flow passages [1, 2].

Results of numerical simulations can give a useful support to experimental work since they allow the analysis of fluid flow and heat transfer phenomena in idealized conditions, where only few selected effects are taken into account. However, due to limited computational resources, the numerical solution of a complete micro heat exchanger has only seldom been carried out [3–5], while detailed simulations of the conjugate convection-conduction heat transfer in microchannel heat exchangers and heat sinks are, in general, only possible with reference to portions of these devices [6]. The part of the device usually considered consists of one or two channels [7–12], but, even in this case, because of the enormous difference between the transverse and the longitudinal scales of the computational domain, the accurate solution of the three-dimensional elliptic form of the Navier-Stokes equations in the portion of the domain corresponding to the flow passages requires a significant CPU time. Therefore, several researchers use simplified approaches where, for instance, a fully developed velocity field or a constant convection coefficient are assumed in the whole microchannel [1, 5, 13], but, of course, this does not allow the entrance effects to be taken into account. In fact, in many duct flows of practical interest for micro heat exchanger design, velocity and temperature fields develop simultaneously, resulting in overlapping hydrodynamic and thermal entrance regions. This occurs when heat transfer begins at the duct inlet, where the velocity boundary layer also starts developing. In such a situation, entrance effects on fluid flow and forced convection heat transfer cannot be neglected if, as it quite often happens in microchannel laminar flows, the total length of the duct is comparable with that of the entrance region.

In this paper, as an alternative to massive CFD, a hybrid technique [14–17], which has the advantage of accounting for all three-dimensional features of the flow field, but with a limited computational effort, is used for the solution of conjugate convection-conduction heat transfer problems in cross-flow micro heat exchangers. A very efficient finite element procedure is first employed for the step-by-step solution of the parabolised momentum equations in a domain corresponding to the cross-sections of the ducts, which are discretized using sufficiently fine grids [18, 19]. Provided that the axial diffusion of momentum can be neglected, such an approach is very advantageous with respect to the one based on the steady-state solution of the elliptic form of the Navier-Stokes equations in a three-dimensional domain corresponding to the whole duct because of the high value of the ratio between the total length and the hydraulic diameter. Then, the three-dimensional hydrodynamically developing velocity field thus determined is used in the finite element solution of the steady-state energy equation in the entire domain, corresponding to both the solid and the fluid parts. Before solving the energy equation, the fulfillment of the discrete mass conservation constraint for the velocity field mapped onto the new grid is obtained by solving a Poisson equation for a velocity correction potential which allows the calculation of appropriate velocity corrections. This technique is standard in the context of fractional step methods, which are often used to solve the continuity and the Navier-Stokes equations [20–22]. While the idea of first solving the Navier-Stokes equation only in the fluid domain corresponding to one microchannel and then the energy equation in both the fluid and solid domains is not new [6, 11, 23, 24], it must be pointed out that the mapping adopted here of the velocity field onto grids with different nodal densities allows a greater flexibility in the meshing of complex geometries.

The above mentioned hybrid approach is applied to the analysis of cross-flow micro heat exchangers consisting of a number of layers of rectangular microchannels stacked one over the other. A parametric study is carried out on the combined effect on cross-flow micro heat exchanger thermal performances due to the variation of the microchannel cross-sections and of the ratio of solid to fluid thermal conductivity. The effects of the heat conduction in the solid walls, which has a strong three-dimensional character, are thus explicitly accounted for. Thermophysical properties of both the solid and the fluids (liquids) are assumed to be constant. Four values of the mass flow rate, three values of the aspect ratio of the rectangular microchannel cross-sections and six values of the solid to fluid thermal conductivity ratio are considered.

STATEMENT OF THE PROBLEM

The following design scenario is considered in this comparative analysis: The mass flow rates of the hot and cold fluids and the total width and height of the micro heat exchanger are fixed, based on design constraints, while the aspect ratio of the rectangular microchannels and the thermal conductivity of the solid material can vary. The type of cross-flow micro heat exchanger considered consists of a number of layers of 10 microchannels each, stacked in such a way that, in each layer, the fluid flows in a direction perpendicular to that of the fluid in the previous and in the following layer, as shown in Fig. 1 with reference to the case of square microchannels. For the sake of simplicity, in this analysis the mass flow rate of the hot fluid is assumend to be equal to that of the cold fluid, and both fluids have the same (constant) thermophysical properties. Moreover, the same mass flow rate

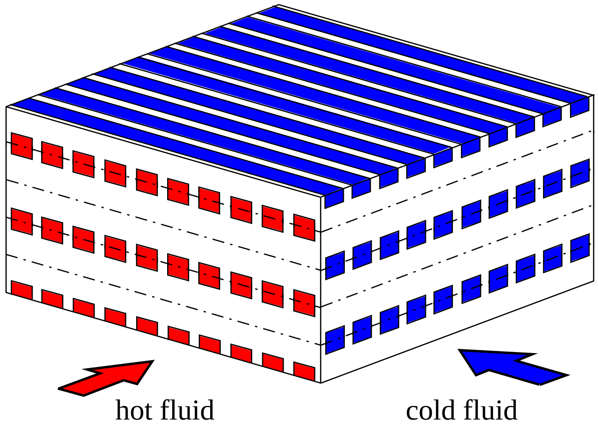

FIGURE 1. Cross-flow micro heat exchanger: sketch of the geometry.

is also assumed in all the microchannels, i.e., there is no fluid maldistribution. The width of all the microchannels is equal to W, while the thicknesses of the solid walls, both between two adjacent microchannels of the same layer and between to adjacent layers, is equal to $W/2$. Thus, the length of the microchannels is $15W$. As far as the microchannel height is concerned, three cases are analyzed here, namely, micro heat exchangers with rectangular microchannels of height H equal to $W/2$, W and $2W$, that is, with cross-section aspect ratios $\gamma = H/W = 0.5$, 1 (square cross-section) and 2, respectively. The corresponding hydraulic diameters are: $0.6667W$, W and $1.3333W$.

MATHEMATICAL MODEL

The following hybrid technique can be employed as an alternative to massive CFD for the solution of steady-state conjugate convection-conduction heat transfer problems in micro heat exchangers where, as in this work, all microchannels are identical and the fluid and the mass flow rate in each microchannel are assumed to be the same. Provided that reference is made to a constant property fluid, that axial diffusion of momentum can be neglected, i.e., the Reynolds number is larger than 50 [25], and that viscous dissipation effects are also negligible, the flow in one of such microchannels is governed by the continuity and the parabolized Navier-Stokes equations, which can be written in the following form

$$\frac{\partial u}{\partial x} + \frac{\partial v}{\partial y} + \frac{\partial w}{\partial z} = 0 \qquad (1)$$

$$\rho_f u \frac{\partial u}{\partial x} = \mu_f \left(\frac{\partial^2 u}{\partial y^2} + \frac{\partial^2 u}{\partial z^2} \right) - \rho_f \left(v \frac{\partial u}{\partial y} + w \frac{\partial u}{\partial z} \right) - \frac{d\overline{p}}{dx} \qquad (2)$$

$$\rho_f u \frac{\partial v}{\partial x} = \mu_f \left(\frac{\partial^2 v}{\partial y^2} + \frac{\partial^2 v}{\partial z^2} \right) - \rho_f \left(v \frac{\partial v}{\partial y} + w \frac{\partial v}{\partial z} \right) - \frac{\partial p}{\partial y} \qquad (3)$$

$$\rho_f u \frac{\partial w}{\partial x} = \mu_f \left(\frac{\partial^2 w}{\partial y^2} + \frac{\partial^2 w}{\partial z^2} \right) - \rho_f \left(v \frac{\partial w}{\partial y} + w \frac{\partial w}{\partial z} \right) - \frac{\partial p}{\partial z} \qquad (4)$$

According to the assumption of a parabolic flow, all the derivatives in the axial direction are neglected in the diffusive terms of Eqs. (2), (3) and (4) [26]. In the above equations, x, y and z are the axial and the transverse Cartesian coordinates, while u, v and w represent the axial and the transverse velocity components. Finally, p is the deviation from the hydrostatic pressure, $\overline{p}$ is its average value over the cross-section, while ρ_f and μ_f, represent density and dynamic viscosity of the fluid, respectively. The two-dimensional solution domain can be bounded by rigid walls or by symmetry axes. On rigid boundaries the no-slip conditions, that is, $u = v = w = 0$, are imposed. Instead, symmetry conditions are either $\partial u/\partial y = \partial w/\partial y = 0$ and $v = 0$, on the symmetry axes parallel to the z-axis, or $\partial u/\partial z = \partial v/\partial z = 0$ and $w = 0$, on those parallel to the y-axis. The model equations are solved using a finite element procedure based on a segregated approach which implies the sequential solution of momentum equations on the two-dimensional domain corresponding to the cross-section of the channel. A marching method is then adopted to move forward in the axial direction, starting from inlet conditions corresponding to a uniform velocity u_i and to $v_i = w_i = 0$ [18]. The pressure-velocity coupling is dealt with using an improved projection algorithm already employed by one of the authors (C.N.) for the solution of the Navier-Stokes equations in their elliptic form [22].

If, as is assumed in this work, all the microchannels in the micro heat exchanger are identical and the fluid and the mass flow rate through each of them is the same, the velocity field, determined for one microchannel by solving Eqs.(1) to (4) on a very fine grid and using a very fine space resolution in the axial direction, can be mapped onto the portions corresponding to the microchannels in the three-dimensional grid which is used to solve the elliptic form of the steady-state energy equation

$$\rho c \left(u \frac{\partial t}{\partial x} + v \frac{\partial t}{\partial y} + w \frac{\partial t}{\partial z} \right) = k \left(\frac{\partial^2 t}{\partial x^2} + \frac{\partial^2 t}{\partial y^2} + \frac{\partial^2 t}{\partial z^2} \right) \qquad (5)$$

in the complete domain of interest, including the fluid in the microchannels and the solid walls. In Eq. (5), t is the temperature and ρ, c and k represent density, specific heat and thermal conductivity, which are equal to ρ_f, c_f and k_f in the fluid and to ρ_s, c_s and k_s in the solid. Obviously, $u = v = w = 0$ are assumed everywhere in the solid. Since this study is mainly aimed at showing the effects of the cross-section aspect ratio and of the ratio of solid to fluid thermal conductivity on micro heat exchanger performances, for the sake of simplicity the solid surfaces at the two ends of the micro heat exchanger where inlets and outlets are located are assumed to be adiabatic, even if this is not completely realistic. Therefore, appropriate boundary conditions on these external solid boundaries are of the Neumann type ($\partial t/\partial n = 0$, where n is the outward normal to the boundary). Instead, symmetry conditions on planes perpendicular to the z-axis are $\partial t/\partial z = 0$. Finally, Dirichlet conditions $t = t_{c,i}$ and $t = t_{h,i}$ are imposed at the inlet boundaries where the cold fluid and the hot fluid enter the domain at temperatures $t_{c,i}$ and $t_{h,i}$, respectively, while Neumann conditions $\partial t/\partial n = 0$ are imposed on outflow boundaries.

As the velocity field is determined before the conjugate thermal problem is solved, the energy equation is the only equation that needs to be solved in a large and complex domain. This, of course, allows significant savings in computer time with respect to a situation where the Navier-Stokes equations also had to be solved in their elliptic form in the same domain and allows significant savings in computer time, thus making systematic studies and optimization procedures easier. However, it must be pointed out that the velocity field mapped onto a coarser grid, whose components can be indicated as u^*, v^* and w^*, in general, does not locally satisfy the discretized continuity equation. Therefore, before solving the energy equation, the appropriate velocity corrections u', v' and w' must be calculated to obtain a corrected velocity field ($u = u^* + u'$, $v = v^* + v'$, $w = w^* + w'$) which satisfies the discretized form of the mass conservation constraint. To this purpose, a technique is employed here, which is standard in the context of fractional step methods, often used to solve the continuity and the Navier-Stokes equations [20–22]. This procedure implies the solution of the discretized form of the Poisson equation for the velocity correction potential ϕ

$$\frac{\partial^2\phi}{\partial x^2} + \frac{\partial^2\phi}{\partial y^2} + \frac{\partial^2\phi}{\partial z^2} = \frac{\partial u^*}{\partial x} + \frac{\partial v^*}{\partial y} + \frac{\partial w^*}{\partial z} \tag{6}$$

subjected to the boundary conditions $\partial\phi/\partial n = 0$ on the whole boundary. In addition, $\phi = 0$ must be specified in an arbitrary point. Then, the nodal values of the velocity corrections u', v' and w' are obtained by solving the discretized forms of the following equations

$$u' = \frac{\partial\phi}{\partial x} \quad ; \qquad v' = \frac{\partial\phi}{\partial y} \quad ; \qquad w' = \frac{\partial\phi}{\partial z} \tag{7}$$

It must be pointed out that, even if, for simplicity, the procedure has been described here on the assumption that all the microchannels in the micro heat exchanger are identical and that the hot and cold fluids have the same thermophysical properties and the same mass flow rate, the proposed hybrid approach is quite general and, with few adaptations, can be easily applied to the case of different fluids, mass flow rates and microchannel sizes. All that is required is a separate solution of Eqs. (1) to (4) for each set of microchannel geometry, thermophysical properties and mass flow rates. Then, the velocity fields thus determined must be appropriately mapped onto the parts of the grid corresponding to the portions of micro heat exchanger being analyzed.

The important components of the procedure illustrated above have already been extensively validated in the past. In particular, the finite element code employed for the solution of the parabolized Navier-Stokes equations has been thoroughly tested and validated through comparisons of calculated results with available literature data [18, 19]. Instead, the code used for the solution of the energy equation in three-dimensional domains is part of a procedure, described in Ref. [27], which also solves the elliptic form of the Navier-Stokes equations and whose validity has been proved in Ref. [28]. Finally, the complete procedure has been validated in Ref. [15] with reference to conjugate convection-conduction problems in circular microchannels with thick walls by comparing axial distributions of the computed wall and bulk temperatures and local Nusselt numbers with those obtained from the solution of the elliptic form of the Navier-Stokes and energy equations with the reliable and thoroughly tested finite element code described in Ref. [27]. An excellent agreement has been found in all cases. The results of these validation tests are not reported here due to lack of space.

NUMERICAL RESULTS

Since, as specified above, in this study the mass flow rates of the hot and cold fluids and the width and height of the micro heat exchanger are assumed to be fixed, the mass flow rate per unit height of micro heat exchanger must remain the same with all the cross-section aspect ratios considered. Four values of the mass flow rate per unit height $\dot{m}'$, namely $\dot{m}' = \dot{m}'_1$, $\dot{m}'_2 = 2\dot{m}'_1$, $\dot{m}'_3 = 4\dot{m}'_1$ and $\dot{m}'_4 = 8\dot{m}'_1$, are selected so that they yield Reynolds numbers $\mathrm{Re} = \rho_f \overline{u} D_h/\mu_f$ typical of microchannel applications and equal to 88.9, 177.8, 355.6 and 711.1 for $\gamma = 0.5$, to 100, 200, 400 and 800 for $\gamma = 1$ and to 111.1, 222.2, 444.4 and 888.9 for $\gamma = 2$. The adopted value of the Prandtl number $\mathrm{Pr} = c_f\mu_f/k_f$ is equal to 5 for both fluids, while six values are assumed for the ratio k_s/k_f of the solid wall to fluid thermal conductivities, namely, $k_s/k_f = 2.5$, 8, 25, 80, 250 and 800. In particular, the first value has been selected to show the behavior of the micro heat exchanger when it is made of a low thermal conductivity material. The third and fifth ones, instead, have been chosen because they are representative of a condition where, if the fluid is water, the micro heat exchanger is made of

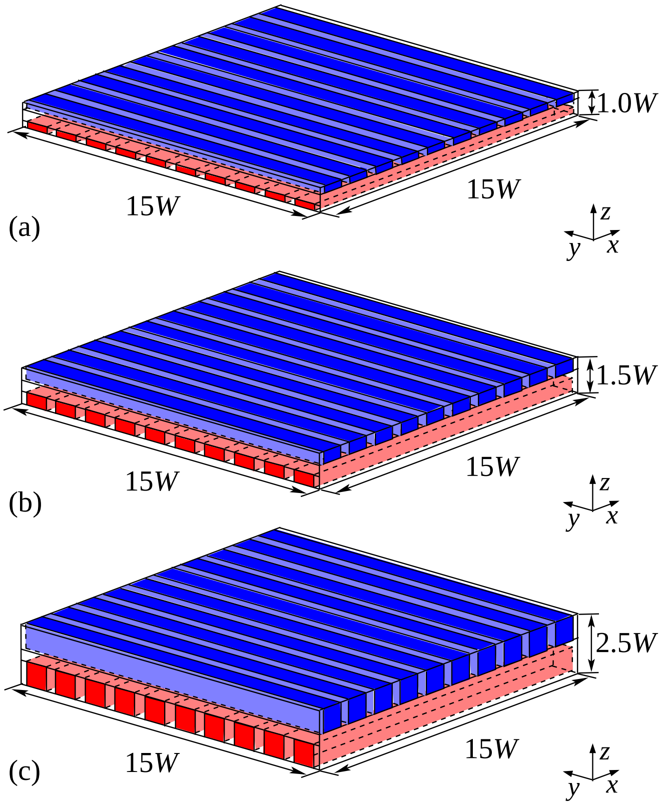

FIGURE 2. Cross-flow micro heat exchanger. Computational domains for microchannel cross-sections with different aspect ratios: (a) $\gamma = 0.5$, (b) $\gamma = 1$ and (c) $\gamma = 2$.

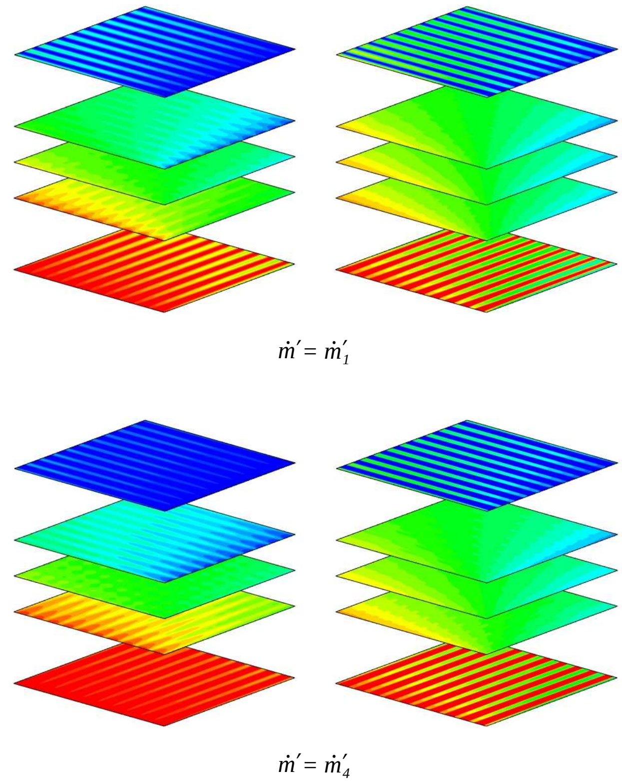

FIGURE 3. Temperature distributions on different planes for $\gamma = 1$ and different mass flow rates (expanded scale in the vertical direction): $k_s/k_f = 2.5$ on the left side, $k_s/k_f = 25$ on the right side.

stainless steel ($k_s/k_f = 25$) or of silicon ($k_s/k_f = 250$). Finally, the last value ($k_s/k_f = 800$) corresponds to the combination silicon–refrigerant fluid.

Only the part of the micro heat exchanger away from the upper and lower external surfaces is analyzed in this study. Therefore, because of the existing symmetries, the computational domains for the three microchannel heights adopted here can be limited to two half-layers of width and length both equal to $15W$ and heights equal to W, $1.5W$ and $2.5W$, as illustrated in Fig. 2. These computational domains are discretized using non-uniform structured meshes of eight-node hexahedral (brick) elements with 240×240 subdivisions in the two horizontal directions. There are 16 subdivisions across each microchannel and 8 subdivisions across each solid wall separating two adjacent flow passages. The number of subdivisions in the vertical direction depends on the cross-section aspect ratio and is equal to 20, 24 and 32 for $\gamma = 0.5$, 1 and 2, respectively, with corresponding total node numbers of $1,219,701$, $1,452,025$ and $1,916,673$.

Each of the two-dimensional domains where the parabolized Navier-Stokes equations are integrated corresponds to one fourth of the cross-section of a single microchannel and is discretized using nonuniform meshes of 30×20, 30×30 and 30×45 bilinear elements for $\gamma = 0.5$, 1 and 2, respectively. The corresponding total numbers of nodes are 651, 961 and $1,426$. The values of the dimensionless step $\Delta x/W$ adopted to march forward in the axial direction range from 1×10^{-4}, at the microchannel inlet, to 1×10^{-2}, at the outlet. Preliminary tests demonstrated that the adopted mesh resolutions and axial steps were adequate to yield nearly grid independent results. Appropriate boundary conditions are applied to take into account that all external solid surfaces are considered adiabatic and that the hot and cold fluids enter the microchannels at temperatures $t_{h,i}$ and $t_{c,i}$, respectively. A typical run to solve the three-dimensional energy equation with the finest of the adopted meshes required between 500 s and 900 s of CPU time on a single core of a recent PC. There are no comparisons with the CPU times necessary to obtain the full solution, i.e., including the Navier-Stokes equations, since the computer resources to solve such a problem on an almost two million node grid were not available.

As a demonstrative example, the temperature distributions on five planes in the computational domain are reported in Fig. 3 with reference to the case of square microchannels ($\gamma = 1$), mass flow rates $\dot{m}'_1$ and $\dot{m}'_4$, and $k_s/k_f = 2.5$ and 25 (expanded scale in the vertical direction). Those for higher values of k_s/k_f are not shown since, in this case, the solid wall is nearly isothermal.

As a further example, to show the effects of the conduction in the solid, the axial distributions of the dimensionless bulk temperature

$$T_{b,c} = \frac{t_{b,c} - t_{c,i}}{t_{h,i} - t_{c,i}} \tag{8}$$

in all the microchannels of the cold layer are reported in Fig. 4 for the two extreme vales of the thermal conductivity ratios and of the mass flow rate per unit height considered here with reference to microchannels of square cross-sections ($\gamma = 1$), namely, $k_s/k_f = 2.5$ and 800, and $\dot{m}' = \dot{m}'_1$ and $\dot{m}'_4$. For a given axial position y/W, higher values of $T_{b,c}$ refer to the microchannels closer to the inlet of the hot fluid. Obviously, higher values of $T_{b,c}$ are obtained for larger values of k_s/k_f and lower values of Re. As expected, for lower values of k_s/k_f, axial conduction effects are not felt much, and the curves are almost straight lines. Obviously, intermediate temperature profiles (not shown here) are yielded by intermediate values of k_s/k_f and Re. Finally, it must be pointed out that, since the heat capacity rates are the same for all the microchannels of both the hot and cold streams, the dimensionless bulk temperatures of the hot fluid is the complement to one of that of the cold fluid in the corresponding microchannel at the same axial distance from the inlet. Similar plots can be obtained for the other geometries.

The minimum and maximum values $(T_{b,c,o})_{min}$ and $(T_{b,c,o})_{max}$ of the dimensionless bulk temperatures $(T_{b,c,o})_j$, with $j = 1, 10$, at the outlet of the microchannels of the cold layer are shown in Fig. 5 for all the cross-section aspect ratios, $\dot{m}' = \dot{m}'_1$ and $\dot{m}'_4$ and different values of k_s/k_f. The temperature difference $(T_{b,c,o})_{max} - (T_{b,c,o})_{min}$ reaches its maximum for intermediate values of the ratio k_s/k_f, since it must tend to zero both for $k_s/k_f \to 0$ (zero flux, i.e., $(T_{b,c,o})_j = 0$ for all the microchannels of the cold layer) and $k_s/k_f \to \infty$ (isothermal walls at $T = (t - t_{c,i})/(t_{h,i} - t_{c,i}) = 0.5$).
The dimensionless average outlet bulk temperature of the whole cold stream

$$\overline{T}_{b,c,o} = \frac{\overline{t}_{b,c,o} - t_{c,i}}{t_{h,i} - t_{c,i}} = \frac{1}{10}\sum_{j=1}^{10}(T_{b,c,o})_j \tag{9}$$

is reported in Fig. 6 as a function of k_s/k_f for all the geometries and mass flow rates considered. It must be pointed out that, in this case, the value of $\overline{T}_{bo}$ coincides with that of the effectiveness

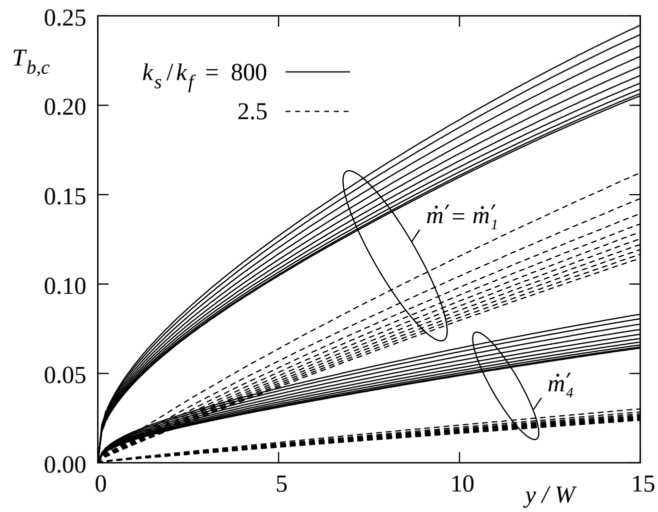

FIGURE 4. Axial distributions of the dimensionless bulk temperature $T_{b,c}$ in different microchannels of the cold layer for $\gamma = 1$, $k_s/k_f = 2.5$ and 800, and $\dot{m}' = \dot{m}'_1$ and $\dot{m}'_4$.

ε of the micro heat exchanger which can be expressed as

$$\varepsilon = \frac{\overline{t}_{b,c,o} - t_{c,i}}{t_{h,i} - t_{c,i}} = \overline{T}_{b,c,o} \tag{10}$$

As can be seen, for $\gamma = 0.5$ and 1 and $\dot{m}' = \dot{m}'_1$, also the effectiveness of the micro heat exchanger reaches a maximum for intermediate values of the ratio k_s/k_f, while for all the other values of γ and $\dot{m}'$ the maximum is attained for $k_s/k_f = 800$. However, in all the cases the effectiveness remains nearly constant for $k_s/k_f \geq 80$.

It is apparent that, for each combination of $\dot{m}'$ and k_s/k_f, the aspect ratio $\gamma = 0.5$ yields the highest effectiveness. However, heat transfer characteristics represent only one of the relevant aspect that must be considered in heat exchanger design, since pressure drop must also be taken into account if one tries to obtain the best overall performance. For each microchannel the total pressure drop can be evaluated as

$$\Delta p = \frac{1}{2}K_i\overline{u}^2 + (\overline{p}_i - \overline{p}_o) + \frac{1}{2}K_o\overline{u}^2 \tag{11}$$

The values $K_i = 0.1$ and $K_o = 1$ are assumed for the resistance coefficients. Of course, since all the microchannels are equal and the hot and cold fluids are assumed to have the same mass flow rates and thermophysical properties, also the pressure drops Δp_h and Δp_c in the hot and cold streams are the same, i.e., we have $\Delta p_h = \Delta p_c = \Delta p$.

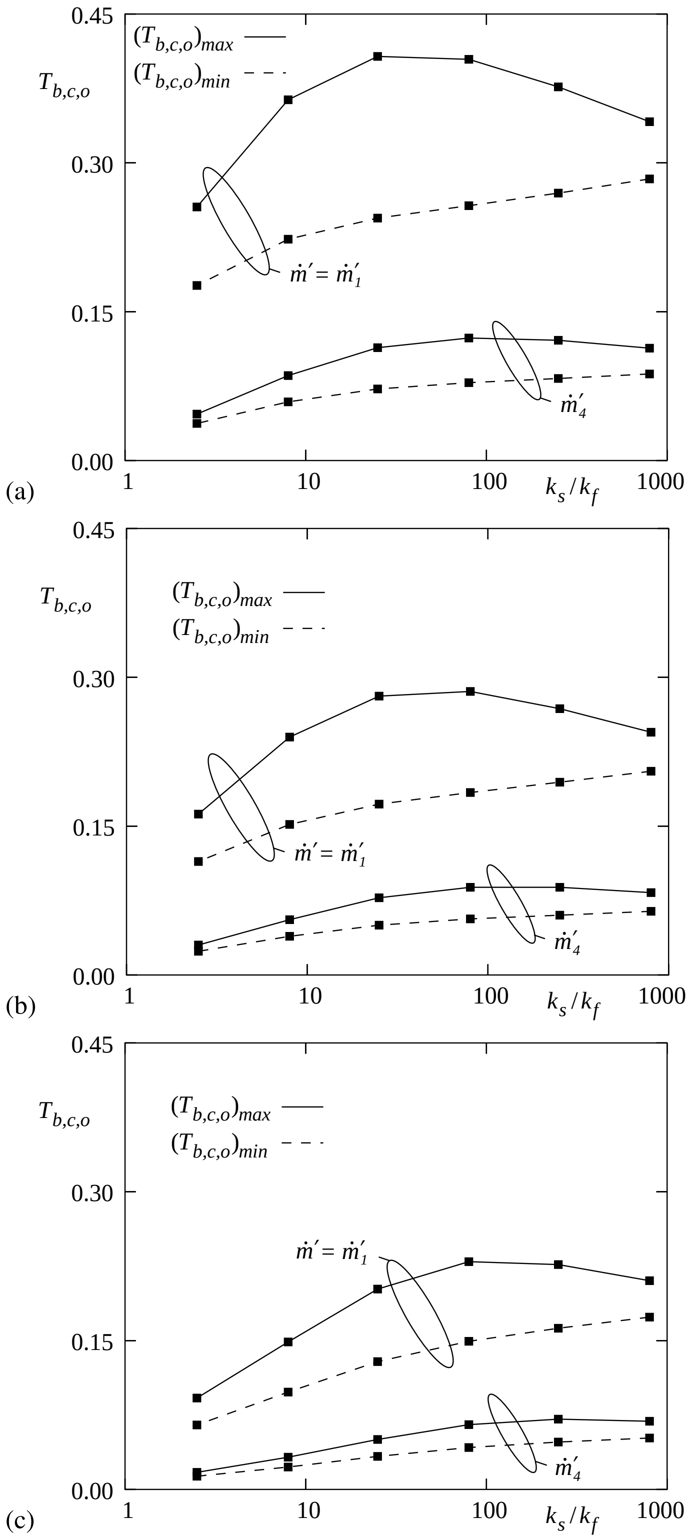

FIGURE 5. Minimum and maximum dimensionless outlet bulk temperature of the cold fluid $T_{b,c,o}$ for $\dot{m}' = \dot{m}'_1$ and $\dot{m}'_4$ and different values of k_s/k_f: (a) $\gamma = 0.5$; (b) $\gamma = 1$; (c) $\gamma = 2$.

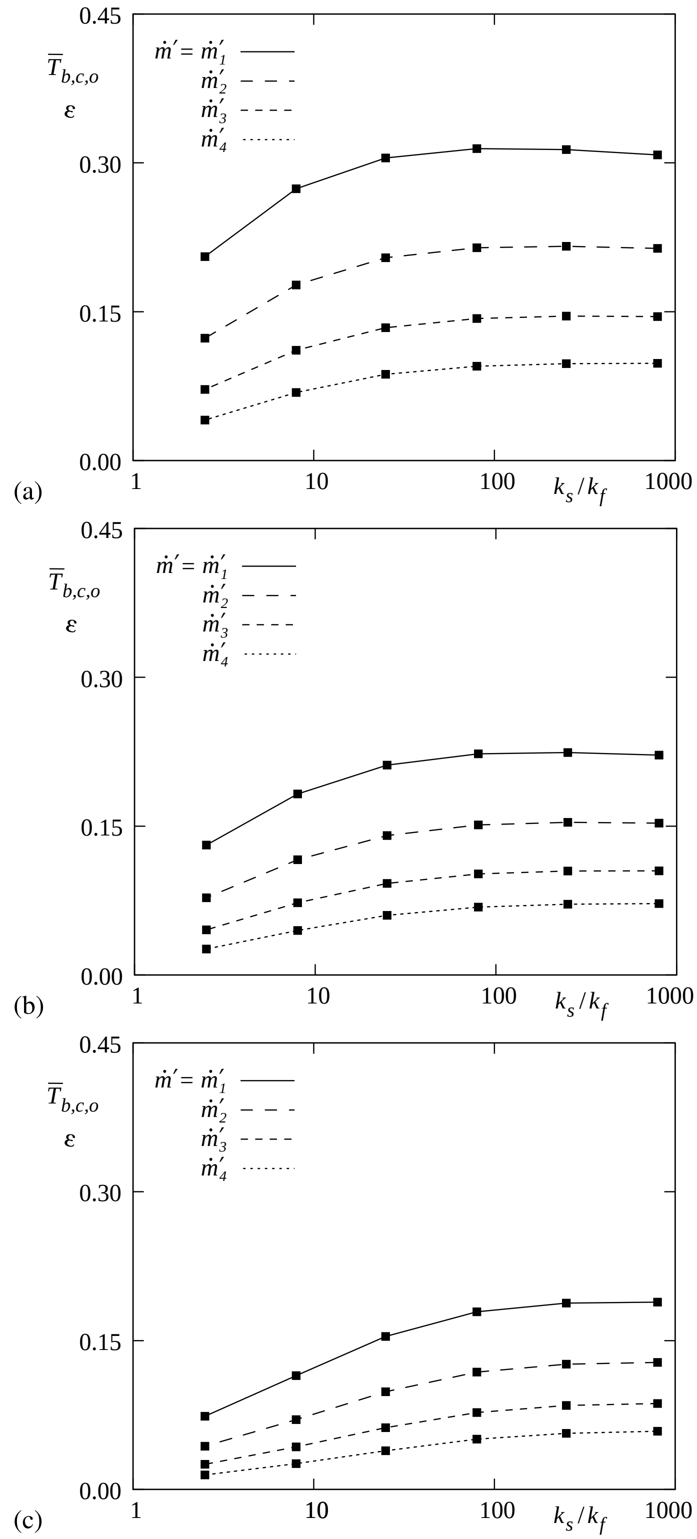

FIGURE 6. Dimensionless average outlet bulk temperature of the whole cold stream and heat exchanger effectiveness for all the values of $\dot{m}'$ and k_s/k_f considered: (a) $\gamma = 0.5$; (b) $\gamma = 1$; (c) $\gamma = 2$.

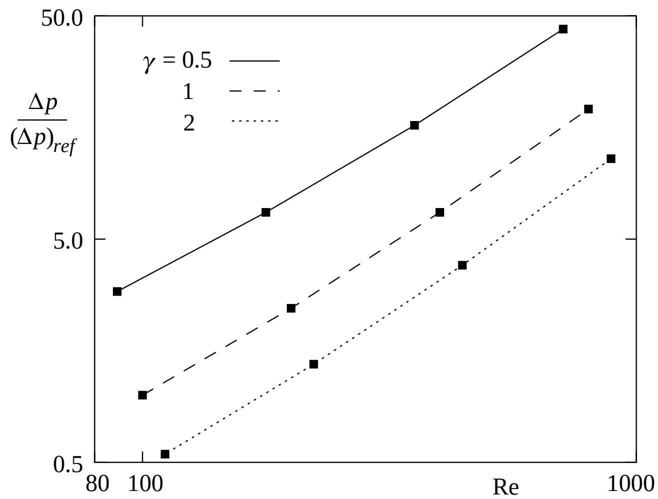

FIGURE 7. Relative pressure drop as a function of the Reynolds number for different micro heat exchanger geometries.

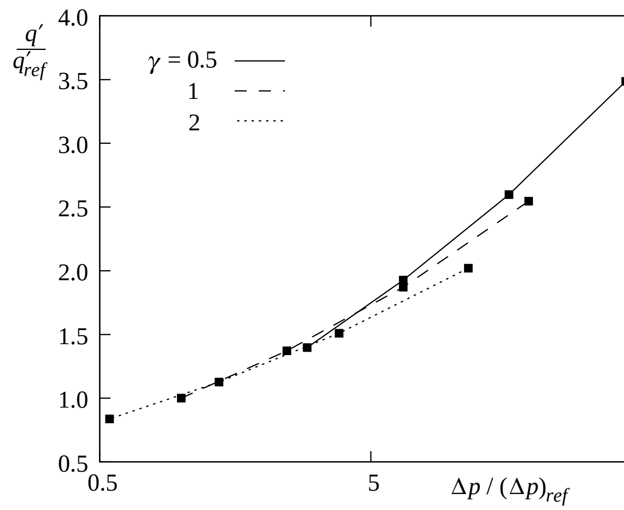

FIGURE 8. Relative heat flow rate per unit height as a function of the relative pressure drop for $k_s/k_f = 250$ and different geometries.

The values of the relative (dimensionless) pressure drop $\Delta p/(\Delta p)_{ref}$, where $(\Delta p)_{ref}$ is the pressure drop in the reference case corresponding to $\gamma = 1$ (square cross-section) and $\dot{m}' = \dot{m}'_1$, are reported in Fig. 7 for the different mass flow rates and microchannel geometries considered. As expected, for each mass flow rate, the larger average axial velocity and the smaller hydraulic diameter pertaining to the micro heat exchanger with $\gamma = 0.5$ yield much lager values of the pressure drop than those obtained with $\gamma = 1$ and $\gamma = 2$.

Finally, in order to assess the overall performances of the considered micro heat exchangers, with reference to each value of the ratio k_s/k_f, the relative (dimensionless) heat flow rate per unit height

$$\frac{q'}{q'_{ref}} = \frac{c\dot{m}'\left(t_{c,i} - \bar{t}_{b,c,o}\right)}{\left[c\dot{m}'\left(t_{c,i} - \bar{t}_{b,c,o}\right)\right]_{ref}} = \frac{\dot{m}'}{\dot{m}'_1}\frac{\left(T_{c,i} - \overline{T}_{b,c,o}\right)}{\left(T_{c,i} - \overline{T}_{b,c,o}\right)_{ref}} \quad (12)$$

can be calculated and plotted as a function of the relative pressure drop. The results obtained for $k_s/k_f = 250$ are shown in Fig. 8. Those pertaining to the other values of k_s/k_f are not reported since they are very similar, both qualitatively and quantitatively. It is apparent in Fig. 8 that for low to moderate values of the relative pressure drop, i.e. low to moderate values of the mass flow rate and Reynolds number, there is no clear advantage in choosing one specific geometry instead of another. However, for larger values of the mass flow rate, higher heat flow rates for a given pressure drop are obtained with lower aspect ratios.

CONCLUSIONS

As an alternative to massive CFD, a hybrid technique, which has the advantage of accounting for all of the three-dimensional features of the flow field, but with a limited computational effort, has been employed for the solution of conjugate convection-conduction heat transfer problems in cross-flow micro heat exchangers consisting of a number of layers of rectangular microchannels. A parametric study has been carried out on the combined effect on cross-flow micro heat exchanger thermal performances due to the variation of the microchannel cross-section and of the ratio of solid to fluid thermal conductivity. In particular, three values of the microchannel cross-section aspect ratio have been considered, namely, 0.5, 1 and 2.

For low to moderate values of the mass flow rate and Reynolds number, heat transfer performances are not significantly influenced by the cross-section aspect ratio, while for larger values the geometries with smaller aspect ratios yield higher heat flow rates for a given pressure drop. As far as the effect of the solid to fluid thermal conductivity ratio is concerned, for values larger than 80, in all the cases considered in this paper, the effectiveness of the micro heat exchanger remains nearly constant.

ACKNOWLEDGMENT

This work was funded by MIUR (PRIN/COFIN 2007 project).

REFERENCES

[1] Maranzana, G., Perry, I., and Maillet, D., 2004. "Mini- and Micro-channels: Influence of Axial Conduction in the

Walls", *Int. J. Heat Mass Transfer*, **47**, pp. 3993-4004.

[2] Hetsroni, G., Mosyak, A., Pogrebnyak, E., and Yarin, L.P., 2005. "Heat Transfer in Micro-Channels: Comparison of Experiments with Theory and Numerical Results", *Int. J. Heat Mass Transfer*, **48**, pp. 5580-5601.

[3] Tiselj, I., Hetsroni, G., Mavko, B., Mosyak, A., Pogrebnyak, E., and Segal, Z., 2004. "Effect of Axial Conduction on the Heat Transfer in Micro-Channels", *Int. J. Heat Mass Transfer*, **47**, pp. 2551-2565.

[4] Kang, M.K., Shin, J.H., Lee, H.-H., and Chun, K., 2005. "Analysis of Laminar Convective Heat Transfer in Micro Heat Exchanger for Stacked Multi-Chip Module", *Microsyst. Technol.*, **11**, pp. 1176-1186.

[5] D'Ortona, U., Luo, A.I., and Tondeur, D., 2001. "A Numerical Study of Cross Flow Compact Heat Exchangers", *Proc. of. CHT'01 Advances in Computational Heat transfer II*, Palm Cove, Australia, Volume 1, pp. 221-228.

[6] Fakheri, A., and Al-Bakhit, H., 2005. "Entrance and Wall Conduction Effects in Parallel Flow Exchangers", *Proc. of the 5th Int. Conf. on Enhanced, Compact and Ultra-Compact Heat Exchangers: Science, Engineering and Technology*, Whistler, Canada, pp. 93-99.

[7] Gamrat, G., Favre-Marinet, M., and Asendrych, D., 2005. "Conduction and Entrance Effects on Laminar Liquid Flow and Hheat Transfer in Rectangular Microchannels", *Int. J. Heat Mass Transfer*, **48**, pp. 2943-2954.

[8] Fedorov, A.G., and Viskanta, R., 2000. "Three-Dimensional Conjugate Heat Transfer in the Microchannel Heat Sink for Electronic Packaging", *Int. J. Heat Mass Transfer*, **43**, 399-415.

[9] Lee, P.-S., Garimella, S.V., and Liu, D., 2005. "Investigation of Heat Transfer in Rectangular Microchannels", *Int. J. Heat Mass Transfer*, **48**, pp. 1688-1704.

[10] Toh, K.C., Chen, X.Y., and Chai, J.C., 2002. "Numerical Computation of Fluid Flow and Heat Transfer in Microchannels", *Int. J. Heat Mass Transfer*, **45**, pp. 5133-5141.

[11] Al-Bakhit, H., and Fakheri, A., 2006. "Numerical Simulation of Heat Transfer in Simultaneously Developing Flows in Parallel Rectangular Ducts", *Applied Thermal Engng.*, **26**, pp. 596-603.

[12] Hasan, M.I., Rageba, A.A., Yaghoubib, M., and Homayoni, H., "Influence of Channel Geometry on the Performance of a Counter Flow Microchannel Heat Exchanger", *Int. J. Thermal Sci.*, **48**, pp. 1607-1618.

[13] Ryu, J.H., Choi, D.H., and Kim, S.J., 2002. "Numerical Optimization of the Thermal Performance of a Microchannel Heat Sink", *Int. J. Heat Mass Transfer*, **45**, pp. 2823-2827.

[14] Nonino, C., Savino, S., Del Giudice, S., and Mansutti, L., 2008. "Solution of Conjugate Forced Convection and Heat Conduction Problems in Microchannel Flows: A Hybrid Approach", *ECI Int. Conf. on Heat Transfer and Fluid Flow in Microscale III*, Whistler, Canada (on CD-ROM).

[15] Nonino, C., Savino, S., Del Giudice, S., and Mansutti, L., 2009. "Conjugate Forced Convection and Heat Conduction in Circular Microchannels", *Int. J. Heat Fluid Flow*, **30**, pp. 823-830.

[16] Nonino, C., Savino, S., and Del Giudice, S., 2008. "Conjugate Forced Convection and Heat Conduction in Micro Heat Exchangers: A Hybrid Approach", *Proc. 1st European Conference on Microfluidics*, Bologna (on CD-ROM).

[17] Nonino, C., Savino, S., and Del Giudice, S., 2009. "A Hybrid Approach to the Numerical Analysis of Cross-Flow Micro Heat Exchangers", *Proc. of the First International Conference on Computational Methods for Thermal Problems*, Naples, Itlay, pp. 117-120.

[18] Nonino, C., Del Giudice, S., and Comini, G., 1988. "Laminar Forced Convection in Three-Dimensional Duct Flows", *Numer. Heat Transfer*, **13**, pp. 451-466.

[19] Nonino, C., Del Giudice, S., and Savino, S., 2006. "Temperature Dependent Viscosity Effects on Laminar Forced Convection in the Entrance Region of Straight Ducts", *Int. J. Heat Mass Transfer*, **49**, pp. 4469-4481.

[20] Patankar, S.K., 1980. *Numerical Heat Transfer and Fluid Flow*, Hemisphere, Washington DC.

[21] Gresho, P.M., 1990. "On the Theory of Semi-Implicit Projection Methods for Viscous Incompressible Flow and its Implementation via a Finite Element Method That Also Introduces a Nearly Consistent Mass Matrix. Part I: Theory", *Int. j. numer. methods fluids*, **11**, pp. 587-620.

[22] Nonino, C., 2003. "A Simple Pressure Stabilization for a SIMPLE-like Equal-Order FEM Algorithm", *Numer. Heat Transfer, Part B*, **44**, pp. 61-81.

[23] Al-Bakhit, H., and Fakheri, A., 2005. "A Hybrid Approach for Full Numerical Simulation of Heat Exchangers", *Proc. of the 2005 ASME Heat Transfer Summer Conference*, San Francisco, CA, U.S.A..

[24] Lelea, D., Nishio, S., and Takano, K., 2004. "The Experimental Research on Microtube Heat Transfer and Fluid Flow of Distilled Water", *Int. J. Heat Mass Transfer*, **47**, pp. 2817-2830.

[25] Shah, R.K., and London, A.L., 1978. *Laminar Flow Forced Convection in Ducts*, Academic Press, New York.

[26] Hirsh, C., 1988. *Numerical Computation of Internal and External Flows*, vol. 1, Wiley, New York.

[27] Nonino, C., and Comini, G., 1997. "An Equal-Order Velocity-Pressure Algorithm for Incompressible Thermal Flows, Part 1: Formulation", *Numerical Heat Transfer - Part B*, **32**, pp. 1-15.

[28] Nonino, C., and Croce, G., 1997. "An Equal-Order Velocity-Pressure Algorithm for Incompressible Thermal Flows, Part 2: Validation", *Numerical Heat Transfer - Part B*, **32**, pp. 17-35.